



## Utilization of inactivated aerobic granular sludge as a potential adsorbent for the removal of sunset yellow FCF

Yanzhuo Zhang, Jun Li\*, Wenjing Li, Guanghui Chen

*The Key Laboratory of Beijing for Water Quality Science & Water Environment Recovery Engineering, The College of Architecture and Civil Engineering, Beijing University of Technology, Beijing 100124, China, Tel. +86 130 1103 0470; email: 83995983@qq.com (Y. Zhang), Tel. +86 136 1124 9208; email: lijunbjut@163.com (J. Li), Tel. +86 131 2476 7843; email: 369443748@qq.com (W. Li), Tel. +86 189 1149 5691; email: 46866221@qq.com (G. Chen)*

Received 5 November 2014; Accepted 2 February 2015

### ABSTRACT

Sunset yellow (SY) FCF is a hazardous azo dye pollutant found in food processing effluents. This study investigates the use of inactivated aerobic granular sludge (AGS) as a potential adsorbent for the removal of SY from water. Adsorption studies were carried out at varying pH values, dosages of adsorbent, initial dye concentrations, and temperatures. Optimal adsorption conditions were identified at pH 2.0, adsorbent dosage of 2.0 g L<sup>-1</sup>, contact time under 120 min, and 35°C temperature. Equilibrium data of the adsorption process fitted very well to the Freundlich model ( $R^2 > 0.99$ ). Kinetics results showed that the experimental data fitted well to the pseudo-second-order model ( $R^2 > 0.99$ ). The thermodynamic parameters such as enthalpy change ( $\Delta H^\circ$ ), entropy change ( $\Delta S^\circ$ ), and Gibbs free energy ( $\Delta G^\circ$ ) were calculated. Thermodynamic testing demonstrated that the adsorption of SY was a spontaneous and endothermic process. Fourier transform infrared spectroscopy indicated that functional groups played an important role during the adsorption of SY. These results confirm that AGS can be used as an adsorbent for successful removal of SY dye from wastewater.

*Keywords:* Adsorption; Sunset yellow FCF; Inactivated aerobic granular sludge; Dyestuff; Kinetic; Isotherm

### 1. Introduction

Dyestuff is commonly used in a variety of industries, such as textiles, paper products, paints, and printing inks. Difficulties inherent to dyestuff removal from wastewater lie in the dye's decolorization and dissociation under light [1]. Azo dyes, universal, organic dyestuffs that come in a wide variety of types, are widely utilized in production of textiles, paper, and leather [2]. The active chemical compounds of the

dyestuff contain one or more functional groups, in which cellulosic fiber (hydroxy), azelon (amino, hydroxyl, and mercaptan groups), and polyamides (amino) combine with oxygen, nitrogen, and sulfur atoms to form covalent links. This combination forms dye with the highest level of color stability. The sizeable discharge loads of azo dyes that has accompanied the rapid development of these industries has quite severely polluted the environment, and urgently requires attention. Azo dyes and products of their decomposition introduce toxicity to aquatic environments, inducing cell mutation that can lead to cancer

\*Corresponding author.

[3]. It is imperative that potential risks of the utilization of these dyestuffs be carefully controlled [4]; specifically, treatment of wastewater containing dyestuff [5].

Sunset yellow (SY) is a type of pyrazolone dyestuff (anionic dye) typically used in food production—beverages, for example, and candies, dairy, and bakery products [1]. Many technologies have been developed previously to treat wastewater containing dyestuff, including biological treatment [6], coagulation/flocculation [7], chemical oxidation [8], membrane filtration [9], ion exchange [10], photocatalytic degradation [11], and adsorption [12]. Adsorption, particularly, is a common and efficient wastewater treatment technology, favored for its convenience and efficiency [13]. Its working principle is the transfer of solute molecules onto the surface of an active adsorbent. Adsorption is superior to other dyestuff removal technologies in terms of low cost, simple design, and convenient operation [14]. Further, the process does not create any harmful byproducts, and a wide range of adsorbents are available for use [4].

Aerobic granular sludge (AGS) is a special biological membrane composed of immobilized cells. Extensive research on application of biological wastewater treatment conducted over the past two decades has shown that biological films are much more effective sewage purifiers than suspended activated sludge [15]. Currently, AGS, a system of immobilized micro-organisms, is a highly promising technology with potential ability to manage high concentrations of organics, nitrogen, phosphorus, and other poisonous or harmful materials in wastewater [15]. AGS effectively adsorbs anionic azo dyestuffs from water solutions, and meets environmental protection requirements. Compared to activated sludge, AGS has higher settlement ability and denser micro-organism structure and porosity [16]. AGS mainly consists of bacteria, protozoa, and extracellular polymeric substance (EPS). The components in the functional groups of bacteria, protozoa, and EPS (e.g. carboxyl, phosphonate, amine, and hydroxyl) form binding sites for the adsorption of dyestuff [15]. No previous study has described the adsorption of SY by AGS, however.

In order to explore novel methods for dyestuff wastewater treatment with AGS, further study of bio-adsorption processes is highly necessary. In this article, laboratory-cultured AGS was used as a raw material which was then pretreated to adsorb anionic SY from water. The adsorption process was optimized by changing different influence factors including pH, dosage of AGS, initial dye concentration, and temperature. Experimental data is detailed in adsorption isotherms, dynamics models, and thermodynamic models.

## 2. Materials and methods

### 2.1. Aerobic granular sludge

The AGS used in the experiment was laboratory-cultured as follows. Activated sludge was collected as seed sludge from an aeration tank at Beijing GaoBeiDian Sewage Treatment Plant, then loaded into a sequencing batch reactor (SBR) for 20 d of preparation. The SBR was cylindrical, had height-to-diameter ratio of 6.5, effective volume of 25 L, 50% of the volume of exchange rate, and water temperature of 25°C. At the beginning of culture, aeration in the SBR was performed using an electromagnetic air pump with air flow rate of 0.2 m<sup>3</sup> h<sup>-1</sup>. Four cycles were run each day of the study. Each period consisted of water-inflow (5 min), aeration (330 min), precipitation (20 min), and drainage (5 min). The material settled gradually over 1 min, alongside the culture-time gradient. The AGS was introduced to synthetic wastewater, the detailed composition of which is shown in Table 1.

After 65 d, the AGS was mature. Its characteristics were as follows: granular size of about 4.0 mm, mass concentration of mixed liquid suspended sludge to inactivate the micro-organisms, the AGS was frozen at -20°C for 10 h. After thawing, the AGS was placed into a beaker then put into a thermostatic water bath at 80°C for 1 h. The AGS maintained physical integrity throughout (Fig. 1(a)).

### 2.2. SY dyestuff

SY, (molecular formula = C<sub>16</sub>H<sub>10</sub>N<sub>2</sub>Na<sub>2</sub>O<sub>7</sub>S<sub>2</sub>, number = 452.37, λ<sub>max</sub> = 482 nm,) is an acid dyestuff. Its pigment ions are negatively charged. SY was prepared as a 1,000 mg L<sup>-1</sup> solution and used as the mother solution in all subsequent experiments. Other reagents used in the experiments were analytic.

### 2.3. Experimental methods

Before adsorption, the AGS was washed three times with distilled water to remove any soluble ions from its surface. Adsorption experiments were carried out at specific temperatures. Appropriate amounts of adsorbent AGS and dyestuff SY solutions were added to an Erlenmeyer flask (capacity 1,000 mg L<sup>-1</sup>), then placed in a constant-temperature shaking incubator (BS-1E, JinTan Medical Instrument, China). The incubator shook at 20°C and at oscillation speed of 150 r min<sup>-1</sup> until reaching adsorption equilibrium. The AGS maintained high granular integrity (Fig. 1(b)).

Table 1  
Compositions of artificial wastewater

Main element	Mass concentration (mL L <sup>-1</sup> )	Trace element	Mass concentration* (mL L <sup>-1</sup> )
NH <sub>4</sub> Cl	192	H <sub>3</sub> BO <sub>3</sub>	150
CH <sub>3</sub> COONa	385	CuSO <sub>4</sub> ·5H <sub>2</sub> O	30
KH <sub>2</sub> PO <sub>4</sub>	10	KI	180
MgSO <sub>4</sub>	8	MnCl <sub>2</sub> ·H <sub>2</sub> O	120
FeSO <sub>4</sub>	1.2	ZnSO <sub>4</sub> ·7H <sub>2</sub> O	120
CaCl <sub>2</sub>	14	CoCl <sub>2</sub> ·6H <sub>2</sub> O	150

\*Trace elements take 0.50 mL L<sup>-1</sup>.

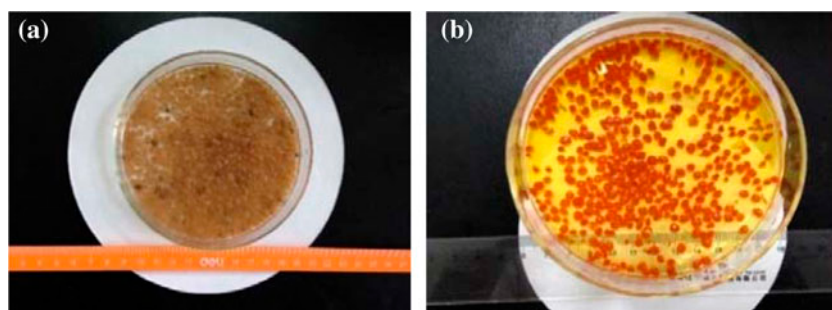


Fig. 1. Images of AGS before and after SY adsorption (a) AGS before SY adsorption and (b) AGS after SY adsorption.

During static adsorption, the pH of the solution was regulated by 1 mol L<sup>-1</sup> HCl and 1 mol L<sup>-1</sup> NaOH. The solution was put into the shaking incubator for 24 h. In order to ensure consistency of all operation steps, the liquid supernatant was assimilated, centrifuged at 3,200 rpm for 2 min, and then measured via ultraviolet spectrophotometry. Adsorbing capacity was determined by comparing dyestuff strengths before and after adsorption.

The effect of pH on the AGS's SY adsorption capacity was investigated in static adsorption experiments. pH ranged between 1.0 and 13.0, AGS dosage was 1.5 g L<sup>-1</sup>, concentration of SY was 150 mg L<sup>-1</sup>, and temperature was 20 °C. The optimal pH value was identified at 2.0, and was maintained throughout subsequent experiments. In order to optimize dosage, AGS dose varied between 0.5 and 2.5 g L<sup>-1</sup>, where concentration of SY was 175 mg L<sup>-1</sup>, and pH was 2. Dosage 2.0 g L<sup>-1</sup> was found to be optimal, and used in subsequent experiments. Initial SY initial concentration varied between 50–250 mg L<sup>-1</sup>, where dosage of AGS was 2.0 g L<sup>-1</sup> and pH was 2. Within the same range of initial SY concentration, adsorption isotherms, and thermodynamic analyses were performed at temperatures between 20–50 °C and adsorption kinetics were performed at 35 °C.

#### 2.4. Analytical methods

The maximum adsorbance wavelength for SY was measured by ultraviolet–visible spectrophotometer (UV-765, Shanghai Precision and Scientific Instrument Co., Ltd.) at 482 nm, and the concentration of dyestuff solution was calculated according to the standard curve. Before and after the adsorption of dyestuff by AGS, Fourier transform infrared (FTIR) spectrometry was recorded by an FTIR meter (Alpha, Infrared Spectrometer Bruker, Germany) under wavelengths from 4,000 to 500 cm<sup>-1</sup>. pH was measured by WTW MTQ/TC2020 meter (Germany).

After adsorption equilibrium was achieved, the adsorbing capacity of SY by AGS was computed as follows:

$$q_e = \frac{V(C_0 - C_e)}{M} \quad (1)$$

where  $q_e$  is the amount of adsorbate adsorbed at the equilibrium (mg g<sup>-1</sup>),  $C_0$  is the initial concentration of SY in solution (mg L<sup>-1</sup>),  $C_e$  is the liquid phase dye concentration at equilibrium (mg L<sup>-1</sup>),  $V$  is the volume of the solution (L), and  $M$  is the mass of the adsorbent used (g).

### 3. Experimental results and discussion

#### 3.1. Factors affecting the adsorption of SY

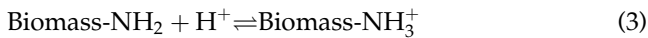
##### 3.1.1. Effect of pH value

Fig. 2(a) shows the relationship between  $q_e$  and pH. The initial concentration of SY was  $150 \text{ mg L}^{-1}$ , the dosage of adsorbent was  $1.5 \text{ g L}^{-1}$ , the temperature was  $20^\circ\text{C}$ , the experimental period was 24 h, and the rate of shaking was 150 rpm in the aqueous solution (Fig. 2(a)).

pH influenced the properties of the sorbent as well as adsorbate speciation. SY was first dissolved, then the sulfonate groups of SY ( $\text{D-SO}_3\text{Na}$ ) were dissociated and converted to anionic dye ions.



With the presence of  $\text{H}^+$ , the amino groups of modified AGS were protonated.



The biosorption process then proceeded due to the electrostatic attraction between these two counter ions.



As shown in Fig. 2(a), from pH 1.0 to 2.0, the adsorption capacity of the AGS was significantly enhanced and  $q_e$  rose from  $81.88$  to  $94.12 \text{ mg g}^{-1}$ . From pH 2 to

12, the adsorption capacity of the AGS was significantly reduced. During the removal of dyestuff via adsorption, pH affects the solubility and coloring characteristics of dyestuffs in wastewater, and also affects the superficial electrification condition of the AGS as well as its decoloration effect. According to Eqs. (2) and (4), the SY dyestuff is first dissolved in an aqueous solution, which sulfonate ( $\text{D-SO}_3\text{Na}$ ) separates and transfers into anions. After acid treatment in the aqueous solution (pH 2), the positive AGS ions are replaced by  $\text{H}^+$ , (protonation of bio-adsorbent.) Finally, the biomass- $\text{NH}_3^+$  with positive charge and the  $\text{D-SO}_3^-$  with negative charge attract each other— This is the primary mechanism by which AGS adsorbs SY dyestuff. Similar conclusions were obtained in a previous study on the removal of hazardous anionic azo dye congo red from wastewater using hen feather [3]. The experiment proved that pH 2 is most effective.

##### 3.1.2. Effect of dosage

Fig. 2(b) shows the effect of adsorbent dosage on  $q_e$  and removal rate. The adsorbent dosage ranged from  $0.5$  to  $3.0 \text{ g L}^{-1}$ , where the initial concentration of SY was  $175 \text{ mg L}^{-1}$  and pH, temperature, experimental time, and shaking rate were unchanged (Fig. 2(b)). The adsorption capacity for SY decreased with increasing dosage of AGS. When the dosage of AGS was low, the removal rate improved with increase in dosage. This occurred likely because with a smaller dosage the space between granules is larger and

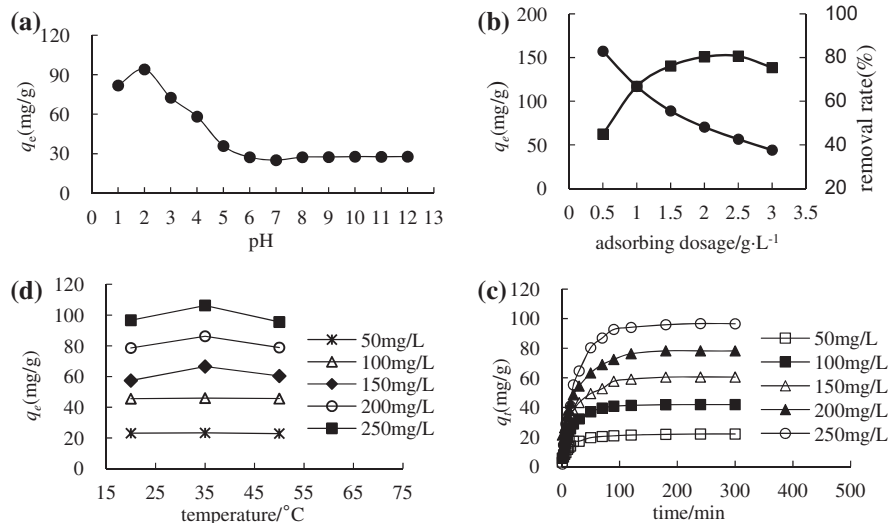


Fig. 2. Effects of (a) pH value, (b) adsorbing rate, (c) initial dye concentration, and (d) temperature on the adsorption of SY by AGS.

relatively more SY molecules aggregate around each granule, facilitating effective surface adsorption, and ion exchange between the AGS and SY. This explains why increased amount of granules forms more adsorption sites for the SY dyestuff, increasing the removal rate. When the concentration of dyestuff increases, its distribution density in the solution reaches a specific level where the space between granules is smaller, the density of valid adsorption points reduces, and the surface adsorption and ion exchange are weakened. These changes combined lead to reduction in adsorbing capacity and removal rate. As previously reported [17], shielding effect is generated around the outskirts of a high-concentration adsorbent, thus preventing the combination of the adsorbate and the adsorption sites and reducing adsorption capacity. Any overlay or blockage of the adsorption sites decreases the adsorbing area, driving the countdown [18]. The experiment showed that the most effective AGS dosage is  $2.0 \text{ g L}^{-1}$ .

### 3.1.3. Effect of initial SY concentration

Fig. 2(c) shows the relationship between  $q_e$  and  $t$  under different initial concentrations of SY. The dosage of the adsorbent was  $2.0 \text{ g L}^{-1}$ , and pH, temperature, experimental time, and shaking rate were unchanged. Most of the SY was removed before 120 min, and adsorption equilibrium was reached at 180 min (Fig. 2(c)). The SY adsorbing rate was highest before 50 min had passed, and slowed after 50 min. The adsorption reached equilibrium rather quickly because adsorption occurred primarily on the surface of the AGS. AGS offers very large superficial area for the adsorption of SY, and provides many opportunities for SY molecules to contact adsorption sites. This quick-to-slow process can also be explained by concentration difference—when the SY was first added, the concentration difference was quite large between the AGS surface and SY molecules in the solution. As time passed, this difference gradually decreased, weakening the adsorption impetus and decreasing the rate of the adsorbing process until reaching equilibrium. In a previous study by Njoku et al. [19], pericarp of rambutan was used to adsorb the dyestuff acid Yellow-17. Similar adsorption curves were obtained regarding the relationship between initial concentration of acid Yellow-17 with  $q_e$  and  $t$ .

### 3.1.4. Effect of temperature

Fig. 2(d) shows that at  $20\text{--}50^\circ\text{C}$ , the relationship between  $q_e$  and the dosage of AGS was  $2.0 \text{ g L}^{-1}$  where

pH, experimental time, and shaking rate were unchanged. As temperature rose,  $q_e$  first increased and then decreased. At lower concentrations ( $50\text{--}100 \text{ mg L}^{-1}$ ), the adsorption capacity was basically the same under different temperatures. Average removal rate under low concentrations was more than 90%, and temperature did not affect the rate much. When the concentration was higher ( $150\text{--}250 \text{ mg L}^{-1}$ ),  $q_e$  at  $35^\circ\text{C}$  was significantly larger than that at  $20$  or  $50^\circ\text{C}$ . As temperature increased, the equilibrium of adsorption capacity first increased and then decreased. This process can be attributed to the fact that the adsorption process is exothermic; thus, as temperature rises, the physical binding force between dyestuff molecules and the adsorbent's functional groups decreases. The solubility of SY increases as the temperature goes up, and the attraction between the solute and the solvent grows stronger than the acting force between the solute and the adsorbent, which complicates the adsorption of the solute [20].

## 3.2. Adsorption isotherms

An adsorption isotherm details the method by which adsorption molecules reach equilibrium during adsorbing processes of both liquid and solid phases. The amount of time required to reach equilibrium is the adsorption time. The balance between adsorbing time and dye adsorption capacity reflects the saturated adsorption capacity of the adsorbent under established operating conditions. Fitting different isothermal adsorption models by data analysis is a crucial step toward determining the model that best fit for the adsorbing process [21].

Three adsorption isotherms, the Langmuir model, Freundlich model, and Dubinin–Radushkevich (D–R) model, were used to fit the experimental data. The applicability of these three isotherm equations was evaluated by coefficient of correlation ( $R^2$ ).

### 3.2.1. Langmuir adsorption isotherm

The assumed prerequisite of the Langmuir adsorption isotherm is that the surfaces of the adsorbent are even, contain a monomolecular layer, and no interaction force exists between the adsorbed molecules [22].

$$\frac{C_e}{q_e} = \frac{C_e}{q_m} + \frac{1}{b \times q_m} \quad (5)$$

In this case,  $q_m$  is the maximum adsorbing capacity ( $\text{mg g}^{-1}$ ), and  $b$  refers to the Langmuir constant ( $\text{L mg}^{-1}$ ).

Table 2  
Constants of adsorption isotherms of SY on AGS at different temperature

parameter	Temperature (°C)		
	20	35	50
Langmuir, the whole concentration range (50–250 mg L <sup>-1</sup> )			
$q_m$ (mg g <sup>-1</sup> )	108.70	142.86	109.89
$b$ (L mg <sup>-1</sup> )	0.0193	0.0115	0.0188
$R^2$	0.9994	0.9982	0.9984
Freundlich, the whole concentration range (50–250 mg L <sup>-1</sup> )			
$K_F$ (mg g <sup>-1</sup> ) (L mg <sup>-1</sup> ) <sup>1/n</sup>	13.57	11.85	13.40
$n^{-1}$	0.46	0.61	0.48
$R^2$	0.9005	0.9426	0.9365
Dubinin-Radushkevich, the whole concentration range (50–250 mg L <sup>-1</sup> )			
$q_m$ (mg g <sup>-1</sup> )	72.44	75.11	80.67
$E$	12.83	13.21	13.98
$R^2$	0.8444	0.8935	0.8548

Experimental data, listed in Table 2, describes the adsorption of SY by AGS at 20, 35, and 50°C used to fit the Langmuir adsorption isotherm. Under concentration of 50–250 mg L<sup>-1</sup>, the experimental data fit the Langmuir adsorption isotherm during the adsorbing process. As shown in Table 2, at temperature of 20–50°C, the  $q_m$  values were 108.70, 142.86, and 109.89 mg g<sup>-1</sup>, among which the  $q_m$  at 35°C was the highest. The  $R^2$  values were 0.9994, 0.9982, and 0.9984 at 20, 35, and 50°C, respectively. The Langmuir adsorption isotherm is suitable to describe the experimental data.

### 3.2.2. Freundlich adsorption isotherm

The Freundlich adsorption isotherm was applied to reveal uneven multilayer adsorption by the adsorbent. The assumed prerequisite is that with increase in adsorbing temperature, the number of adsorption sites increases exponentially [23].

$$\ln q_e = \ln K_F + \frac{1}{n} \ln C_e \quad (6)$$

where  $K_F$  is the Freundlich constant, and  $n$  is the Freundlich exponent.

The Freundlich model fitted linearly to the experimental data which describes the adsorption of SY by AGS at 20, 35, and 50°C. The results of  $K_F$ ,  $n^{-1}$ , and  $R^2$  are listed in Table 2. With concentration of 50–250 mg L<sup>-1</sup>, the  $n^{-1}$  values of the Freundlich model were all less than one (Table 2). The  $R^2$  values were 0.9637, 0.9912, and 0.9834 under the three tested temperatures. When  $n^{-1}$ , which measure the uneven adsorption

strength or the surface [24], ranged from 0 to 1, surface adsorption was facilitated quite easily. The  $R^2$  values of the Freundlich model were smaller than those of the Langmuir model. The experimental data lie within the concentration range, but the Freundlich deviated from the trend line. The experimental results showed that the Freundlich adsorption isotherm, which was used to describe the polymolecular layer, did not fit the data. The Freundlich adsorption isotherm showed that the activation energies carried by surface groups toward various adsorption reactions were different, and that the adsorption reaction occurred at different adsorption sites, such as amido, carboxyl, or hydroxyl sites [25]. (This conclusion is consistent with the results of the infrared spectroscopy discussed below.)

### 3.2.3. Dubinin–Radushkevich (D–R) adsorption isotherm

The D–R adsorption isotherm is based on the theory of micropore filling, and can be used to describe the adsorbing process on even or uneven surfaces [26]. The linear form of the D–R equation is expressed as follows:

$$\ln q_e = \ln q_m - \beta \varepsilon^2 \quad (7)$$

where  $q_m$  is the D–R capacity of a monomolecular layer (mg g<sup>-1</sup>),  $\beta$  is the activity coefficient related to adsorption mean free energy (mol<sup>2</sup>J<sup>-2</sup>), and  $\varepsilon$  is the equilibrium concentration potential related to Polanyi (J mol<sup>-1</sup>), which is expressed as follows:

$$\varepsilon = RT \ln \left( 1 + \frac{1}{C_e} \right) \quad (8)$$

where  $R$  is a gas constant 8.314 J (mol K)<sup>-1</sup>,  $T$  is the absolute temperature (K), and  $E$  is the average free energy (J mol<sup>-1</sup>). The relationship between  $E$  and  $\beta$  can be described as follows:

$$E = (2\beta)^{-0.5} \quad (9)$$

The D–R model was fitted to the experimental data linearly to describe the adsorption of SY by AGS at 20–50°C. According to Eqs. (7) and (9), whether the adsorption process was primarily physical or chemical can be determined by fitting the D–R model with experimental data. At the micro-level, the D–R model is a much more popular isotherm adsorption model than the Langmuir model, as its derivation is not

based on an ideal assumption, (such as that adsorption sites are even, there is no steric hindrance during the ionic adsorption, or that the surfaces are even [27].) When average free energy  $E$  was 8–16 kJ mol<sup>-1</sup>, chemical adsorption dominated; if  $E < 8$  kJ mol<sup>-1</sup>, physical adsorption did (Table 2). For this experiment, the values of  $E$  at 20, 35, and 50 °C were 12.83, 13.21, and 13.98, respectively, which indicates that chemical adsorption is dominant in the adsorption of SY by AGS.

### 3.3. Adsorption kinetics

To better describe the adsorption process, explain the reaction process, and determine the control principles from the perspective of kinetics, various kinetic models are built as follow. The primary models include pseudo-first-order kinetics, pseudo-second-order kinetics, and internal diffusion kinetics, used here to study the reaction pathway and rate-control step during the adsorption of SY by AGS.

#### 3.3.1. Pseudo-first-order kinetic model

The pseudo-first-order kinetic model was first presented by Lagergren to study the adsorbing process of liquid-phase to solid-phase systems [28], expressed as follows:

$$\log(q_e - q_t) = \log q_e - \frac{k_1 t}{2.303} \quad (10)$$

where  $q_t$  is the amount of dye adsorbed at time  $t$  (mg g<sup>-1</sup>), and  $k_1$  is the pseudo-first-order rate constant (min<sup>-1</sup>).

Fig. 3(a) shows the relationship between  $\log(q_e - q_t)$  and  $t$  under different pH and initial dyestuff concentrations. The constant,  $k_1$ , can be calculated from the isothermal straight slope and intercept. As shown in Table 3,  $q_{e,cal}$  was much smaller than  $q_{e,exp}$  and  $R^2$  lay between 0.6555 and 0.9910, indicating that the experimental data did not fit the pseudo-first-order kinetic model. To this effect, this model does not describe the entire adsorbing process, but is applicable to the primary stage of the adsorption process [29].

#### 3.3.2. Pseudo-second-order kinetic model

The pseudo-second-order kinetic model was first proposed by Ho and McKay to conduct complete analysis of kinetic data [30]. The model is expressed as follows:

$$\frac{t}{q_t} = \frac{1}{k_2 q_e^2} + \frac{t}{q_e} \quad (11)$$

where  $q_t$  is the amount of dye adsorbed at time  $t$  (mg g<sup>-1</sup>) and  $k_2$  is the pseudo-second-order rate constant (g (mg min)<sup>-1</sup>).

Fig. 3(b) shows the relation between  $t/q_e$  and  $t$  under different pH and different initial dyestuff concentrations. The constant,  $k_2$ , can be calculated from

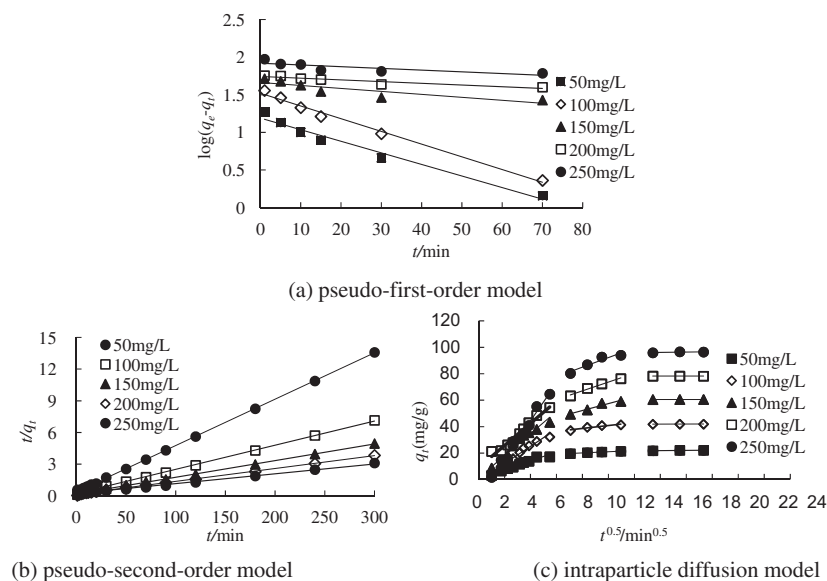


Fig. 3. Kinetic models for adsorption of SY by AGS at different initial concentration.

Table 3  
Kinetic model parameters for adsorption of SY by AGS at different initial concentration

Dye	C <sub>0</sub>	Pseudo-first-order kinetics			Pseudo-second-order kinetics			q <sub>e,exp</sub> (mg g <sup>-1</sup> )	Intraparticle diffusion kinetics		
		q <sub>e,cal</sub> (mg g <sup>-1</sup> )	k <sub>1</sub> (min <sup>-1</sup> )	R <sup>2</sup>	q <sub>e,cal</sub> (mg g <sup>-1</sup> )	k <sub>2</sub> (g (mg min) <sup>-1</sup> )	R <sup>2</sup>		k <sub>3</sub> (mg g <sup>-1</sup> min <sup>-1/2</sup> )	C	R <sup>2</sup>
SY	50	3.28	1.71	0.9736	26.46	0.53	0.9999	23.33	0.44	16.58	0.9824
	100	4.57	2.08	0.9910	54.95	0.23	0.9994	46.00	1.10	9.84	0.8968
	150	5.27	2.28	0.7602	80.65	0.14	0.9993	66.51	2.64	31.05	0.9395
	200	5.72	2.42	0.8845	98.04	0.09	0.9988	88.23	3.31	40.56	0.9847
	250	6.81	2.54	0.6555	119.05	0.04	0.9957	106.27	3.63	55.98	0.9140

the isothermal straight slope and intercept. As shown in Table 3,  $q_{e,cal}$  was quite close to  $q_{e,exp}$ , and the values were basically the same.  $R^2$  was between 0.9957 and 0.9999, which indicates high correlation. The pseudo-second-order kinetic model was thus much more appropriate for fitting the experimental data. Comparison between the two showed that chemical adsorption was the rate-controlling step during the adsorption of SY by AGS. These results indicate that chemical groups were at work between SY molecules and the surface of the AGS, and that SY dyestuff molecules were mainly adsorbed onto the surface of the AGS.

### 3.3.3. Intraparticle diffusion model

Adsorption kinetics involves various adsorbing mechanisms, where one major restriction is the diffusion mechanism. The diffusion mechanism cannot be determined by pseudo-first- or pseudo-second-order kinetic models, but was analyzed by internal granular diffusion kinetic model [31]. The equation is expressed as follows:

$$q_t = k_3 t^{0.5} + C \quad (12)$$

where  $k_3$  is the rate constant of intraparticle diffusion (mg g<sup>-1</sup> min<sup>-0.5</sup>),  $t^{0.5}$  is the half-life time in seconds, and  $C$  is the intercept proportional to the boundary layer thickness.

Fig. 3(c) shows the intraparticle diffusion model of SY dyestuff under different initial concentrations. This multi-linear curve shows that several individual steps occurred during the entire adsorbing process. The curve can be divided into three parts: straight-up, slow-rise, and smooth-steady. During the first part, SY diffused rapidly around the superficial, thin layer of the AGS (membrane diffusion). During the second part, SY diffused inside the adsorbent granules

(in-granule diffusion). During the third part, the adsorption reached equilibrium.  $k_3$  and  $C$  are indicated by the data of the second part.

The fitting performance of the figure lines was high.  $R^2$  was between 0.8969 and 0.9847, demonstrating that experimental data was described successfully by the intraparticle diffusion model. Because the second part does not pass the original point, the inside-adsorbent diffusion of AGS is considered the controlling step during the adsorbing process. (Membrane diffusion was also another controlling step, however.) The constant,  $k_3$ , and the intercept,  $C$ , were also analyzed. Table 3 shows that  $k_3$  and  $C$  both increased as the initial concentration improved to optimal conditions, which indicates that the internal diffusion rate increased with increase in initial concentration. Increase in initial concentration led to higher concentration gradient, and finally to quicker diffusion and adsorption. When  $C$  increased,  $k_3$  was higher, which indicates that increased boundary layer thickness affect the adsorption by creating greater effect on the boundary layer [18]. A similar situation occurs in the adsorption activated carbon, (the main material of which is staminate flowers of coconut trees,) used on SY [32].

### 3.4. Adsorption thermodynamics

Thermodynamic parameters are important indicators of the effectiveness of an adsorbing process. These include  $\Delta H^\circ$ ,  $\Delta S^\circ$ , and  $\Delta G^\circ$ , expressed as follows:

$$\ln K_d = \frac{\Delta S^\circ}{R} - \frac{\Delta H^\circ}{RT} \quad (13)$$

$$K_d = \frac{q_e}{C_e} \quad (14)$$

$$\Delta G^\circ = \Delta H^\circ - T\Delta S^\circ \quad (15)$$

Table 4  
Thermodynamic parameters of SY adsorption by AGS

$C_0$ (mg L <sup>-1</sup> )	$\Delta G^\circ$ (kJ mol <sup>-1</sup> )			$\Delta H^\circ$ (kJ mol <sup>-1</sup> )	$\Delta S^\circ$ (J (mol K) <sup>-1</sup> )
	293 K	308 K	323 K		
50	-4.42	-4.90	-4.53	-4.13	1.58
100	-3.99	-4.40	-4.46	-0.61	14.18
150	-1.19	-3.44	-1.94	-2.21	14.36
200	-1.48	-2.88	-1.68	-2.14	7.42
250	-1.30	-2.63	-1.29	-3.80	5.22

According to Table 4, at 293, 303, and 323 K, the values of  $\Delta G^\circ$  and  $\Delta H^\circ$  were all negative, indicating that the adsorption is likely a spontaneous, exothermic process. This is consistent with the conclusion of former experimental data, which showed that  $q_e$  first increased then decreased alongside temperature rise. If  $\Delta S^\circ$  is positive during the adsorbing process, the interface between solid and liquid phases grows more complex. Positive  $\Delta S^\circ$  value reflects the dyestuff's strong attraction toward the AGS [33]. In this experiment, under 50–250 mg L<sup>-1</sup>, the values of  $\Delta S^\circ$  were all positive. This indicates that over the entire concentration range, AGS showed high adsorption affinity for SY. In summary, the adsorption of SY by AGS is a spontaneous, exothermic process.

### 3.5. FTIR analysis

Fig. 4 shows the FTIR spectra before and after adsorption of SY by AGS. During the adsorption process, changes in peak at 3,442 and 3,167 cm<sup>-1</sup> after adsorption, and at 3,443 and 3,138 cm<sup>-1</sup> before adsorption, may be attributed to the stretching vibration of N–H and of O–H in alcohol. The before–after change

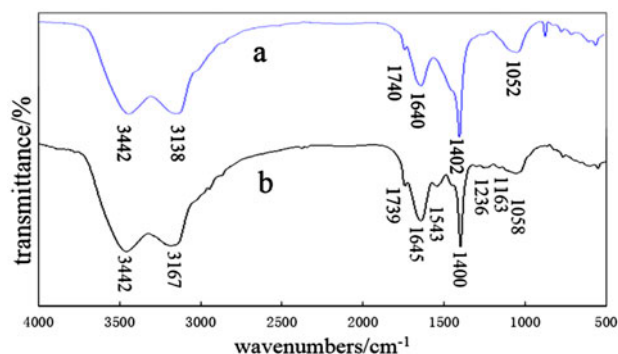


Fig. 4. FTIR spectra of granular sludge: (a) before SY adsorption, and (b) after SY adsorption.

at 1,740 and 1,739 cm<sup>-1</sup> was likely created by the stretching vibration of C=O in aliphatic series. The before-adsorption peak at 1,640 cm<sup>-1</sup> and the after-adsorption peak at 1,645 cm<sup>-1</sup> are quite obvious, and were probably caused by the combination of the stretching vibration of in-protein C=O (amide I band) and the flexural vibration of N–H (amide II band). A new after-adsorption peak appears at 1,543 cm<sup>-1</sup>, most likely caused by the interaction between the flexural vibration of in-protein N–H (amide II band) with the stretching vibration of C–N in the C–N–H group. Peaks of different degrees occur near 1,400 cm<sup>-1</sup> after adsorption and at 1,402 cm<sup>-1</sup> before adsorption, which originate from the stretching vibration of C–O and the flexural vibration of O–H Key. New peaks appear at 1,236 and 1,163 cm<sup>-1</sup> after adsorption, probably caused by the stretching vibration of C–O in alcohol. The peaks at 1,052 and 1,058 cm<sup>-1</sup> both before and after adsorption are likely due to the interaction between the stretching vibrations of O–H in polysaccharide and C–O in alcohol.

Compared to peaks at 3,442 and 3,138 cm<sup>-1</sup> before adsorption, the peaks at 3,442 and 3,167 cm<sup>-1</sup> after adsorption were wider, probably due to the changes of bond energies caused by stretching vibration of N–H and of O–H in alcohol. Compared to the peak at 1,645 cm<sup>-1</sup> after adsorption, the peak at 1,640 cm<sup>-1</sup> was sharper and slightly transferred, which shows that protein and SY dyestuff joined in the adsorbing process and reacted. Compared to the peak at 1,402 cm<sup>-1</sup> after adsorption, the peak at 1,400 cm<sup>-1</sup> after adsorption was weakened, caused by the stretching vibration of C–O and the flexural vibration of O–H Key. This result further indicates that groups such as amide I (peptide bond of protein), carboxyl, alcohol, and phenol (humus acid group) participated in the adsorbing process. Compared to the peak at 1,058 cm<sup>-1</sup> after adsorption, the characteristic peak at 1,052 cm<sup>-1</sup> transferred slightly, which indicates that both O–H in polysaccharide and C–O in alcohol took part in the adsorbing process.

AGS is mainly comprised of bacteria, protozoon, and EPS. The outer cell membrane of bacteria, eukaryotic cells of protozoa, and EPS are primarily composed of proteins, lipids, polysaccharides, and nucleic acids. The organic compounds group of the AGS, which includes carboxylic acid (–COOH), aldehyde (–COH), hydroxyl (–CHOH), sulfhydryl (–SH), phosphoryl group (–PO<sub>4</sub>H<sub>3</sub>), and amine (–NH<sub>2</sub>), joins with dyestuff molecules in the liquid-phase [34,35]. FTIR analysis showed that the main functional groups of AGS adsorption toward SY dyestuff were amido, oxhydryl, carboxyl, groups of sulfur, and phosphorus.

#### 4. Conclusion

Notable conclusions can be summarized as follows.

- (1) The pH of the solution was an important factor affecting AGS adsorption of SY dyestuff. Anionic SY was adsorbed better under acidic conditions (pH 2), and with higher concentration of  $H^+$ , more functional groups on the cytomembrane surface of AGS appeared. This result was consistent with the FTIR spectra, where the amount of peaks after adsorption was greater than that before adsorption. Adsorbing capacity reached its optimal level when the dosage of AGS was  $2\text{ g L}^{-1}$ , the temperature was  $35^\circ\text{C}$ , and pH was 2.  $q_e$  increased as initial SY concentration increased.
- (2) Comparing  $R^2$  values, the Langmuir isotherm fit experimental data more aptly than the Freundlich isotherm or D–R isotherm. The D–R isotherm indicated that chemical adsorption was dominant during the adsorption of SY by AGS.
- (3) The adsorbing process of AGS acting on SY dyestuff fits the pseudo-second-order kinetic model ( $R^2 > 0.9900$ ). The intraparticle diffusion model showed that membrane diffusion and internal diffusion were both present in AGS's SY adsorption process.
- (4) During the adsorbing process the measured values of  $\Delta G^\circ$  were all negative, which indicates the process was spontaneous. The values of  $\Delta H^\circ$  were all negative, which additionally indicates that the adsorbing process was exothermal. This result was consistent with former experimental data, in that equilibrium adsorption capacity was improved with increased temperature. Values of  $\Delta S^\circ$  in the entire concentration were positive, which indicates SY's affinity toward AGS.
- (5) FTIR analysis showed that the functional groups of AGS play a crucial role during the SY adsorption process. Functional groups (amido, carboxyl, hydroxyl, sulfur, and phosphorus,) were the active adsorption sites. Over the course of the experiment, the AGS effectively removed the SY dyestuff from the aqueous solution, indicating the feasibility of AGS as a low-cost adsorbent and creating a foundation for further study on the adsorption of dyestuffs.

#### Acknowledgments

The work was supported by the Critical Patented Project of the Control and Management of National Polluted Water Bodies (2014ZX07201-011), and the Natural Science Foundation of Beijing (8122005).

#### References

- [1] M. Ghaedi, A. Hekmati Jah, S. Khodadoust, R. Sahraei, A. Daneshfar, A. Mihandoost, M.K. Purkait, Cadmium telluride nanoparticles loaded on activated carbon as adsorbent for removal of sunset yellow, *Spectrochim. Acta A*. 90 (2012) 22–27.
- [2] A.A. Ahmad, B.H. Hameed, Fixed-bed adsorption of reactive azo dye onto granular activated carbon prepared from waste, *J. Hazard. Mater.* 175 (2010) 298–303.
- [3] A. Mittal, V. Thakur, J. Mittal, H. Vardhan, Process development for the removal of hazardous anionic azo dye Congo red from wastewater by using hen feather as potential adsorbent, *Desalin. Water Treat.* 52 (2014) 227–237.
- [4] J. Mittal, D. Jhare, H. Vardhan, A. Mittal, Utilization of bottom ash as a low-cost sorbent for the removal and recovery of a toxic halogen containing dye eosin yellow, *Desalin. Water Treat.* 52 (2013) 1–12.
- [5] H.J. Gao, T.T. Kan, S.Y. Zhao, Y.X. Qian, X.Y. Cheng, W.L. Wu, X.D. Wang, L.Q. Zheng, Removal of anionic azo dyes from aqueous solution by functional ionic liquid cross-linked polymer, *J. Hazard. Mater.* 261 (2013) 83–90.
- [6] L.C. Apostol, L. Pereira, R. Pereira, M. Gavrilesco, M.M. Alves, Biological decolorization of xanthene dyes by anaerobic granular biomass, *Biodegradation* 23 (2012) 725–737.
- [7] S. Sadri Moghaddam, M.R. Alavi Moghaddam, M. Arami, Coagulation/flocculation process for dye removal using sludge from water treatment plant: Optimization through response surface methodology, *J. Hazard. Mater.* 175 (2010) 651–657.
- [8] O. Türgan, G. Ersöz, S. Atalay, J. Forss, U. Welander, The treatment of azo dyes found in textile industry wastewater by anaerobic biological method and chemical oxidation, *Sep. Purif. Technol.* 79 (2011) 26–33.
- [9] D.E. Zavastin, S. Gherman, I. Cretescu, Removal of direct blue dye from aqueous solution using new polyurethane–cellulose acetate blend micro-filtration membrane, *Rev. Chim.* 63 (2012) 1075–1078.
- [10] M. Naushad, A. Mittal, M. Rathore, V. Gupta, Ion-exchange kinetic studies for Cd(II), Co(II), Cu(II), and Pb(II) metal ions over a composite cation exchanger, *Desalin. Water Treat.* (2014) 1–8.
- [11] P. Madhusudan, J. Zhang, B. Cheng, G. Liu, Photocatalytic degradation of organic dyes with hierarchical  $\text{Bi}_2\text{O}_2\text{CO}_3$  microstructures under visible-light, *Cryst. Eng. Comm.* 15 (2012) 231–240.
- [12] H. Daraei, A. Mittal, M. Noorisepehr, F. Daraei, Kinetic and equilibrium studies of adsorptive removal of phenol onto eggshell waste, *Environ. Sci. Pollut. Res.* 20 (2013) 4603–4611.

- [13] M. Rafatullah, O. Sulaiman, R. Hashim, A. Ahmad, Adsorption of copper (II), chromium (III), nickel (II) and lead (II) ions from aqueous solutions by meranti sawdust, *J. Hazard. Mater.* 170 (2009) 969–977.
- [14] J. Mittal, V. Thakur, A. Mittal, Batch removal of hazardous azo dye Bismark Brown R using waste material hen feather, *Ecol. Eng.* 60 (2013) 249–253.
- [15] S.S. Adav, D.J. Lee, K.Y. Show, J.H. Tay, Aerobic granular sludge: Recent advances, *Biotechnol. Adv.* 26 (2008) 411–423.
- [16] J.F. Gao, Q. Zhang, K. Su, R.N. Chen, Y.Z. Peng, Biosorption of Acid Yellow 17 from aqueous solution by non-living aerobic granular sludge, *J. Hazard. Mater.* 174 (2010) 215–225.
- [17] A. Mittal, Removal of the dye, amaranth from waste water using hen feathers as potential adsorbent, *Electron. J. Environ. Agric. Food Chem.* 5 (2006) 1296–1305.
- [18] H. Daraei, A. Mittal, J. Mittal, H. Kamali, Optimization of Cr(VI) removal onto biosorbent eggshell membrane: Experimental & theoretical approaches, *Desalin. Water Treat.* 52 (2014) 1307–1315.
- [19] V.O. Njoku, K.Y. Foo, M. Asif, B.H. Hameed, Preparation of activated carbons from rambutan (*Nephelium lappaceum*) peel by microwave-induced KOH activation for acid yellow 17 dye adsorption, *Chem. Eng. J.* 250 (2014) 198–204.
- [20] G. Crini, P.M. Badot, Application of chitosan, a natural aminopolysaccharide, for dye removal from aqueous solutions by adsorption processes using batch studies: A review of recent literature, *Prog. Polym.* 33 (2008) 399–447.
- [21] R. Jain, P. Sharma, S. Sikarwar, J. Mittal, D. Pathak, Adsorption kinetics and thermodynamics of hazardous dye Tropaeoline 000 onto Aeroxide Alu C (Nano alumina): A non-carbon adsorbent, *Desalin. Water Treat.* 52 (2013) 1–8.
- [22] M. Manshour, H. Daraei, A.R. Yazdanbakhsh, A feasible study on the application of raw ostrich feather, feather treated with H<sub>2</sub>O<sub>2</sub> and feather ash for removal of phenol from aqueous solution, *Desalin. Water Treat.* 41 (2012) 179–185.
- [23] H. Daraei, A. Mittal, M. Noorisepehr, J. Mittal, Separation of chromium from water samples using eggshell powder as a low-cost sorbent: Kinetic and thermodynamic studies, *Desalin. Water Treat.* (2013) 1–7.
- [24] A. Mittal, L. Kurup, Column operations for the removal & recovery of a hazardous dye 'Acid Red - 27' from aqueous solutions, using waste materials—Bottom ash and de-oiled soya, *Ecol. Environ. Conserv.* 13 (2006) 181–186.
- [25] Y.C. Wong, Y.S. Szeto, W.H. Cheung, G. McKay, Equilibrium studies for acid dye adsorption onto chitosan, *Langmuir* 19 (2003) 7888–7894.
- [26] M.M. Dubinin, L.V. Radushkevich, Equation of the characteristic curve of activated charcoal, *Chem. Zentr.* 1 (1947) 875.
- [27] M.P. Jian, C.C. Tang, M. Liu, Adsorptive removal of Cu<sup>2+</sup> from aqueous solution using aerobic granular sludge, *Desalin. Water Treat.* (2014) 1–10.
- [28] Q. Sun, L.Z. Yang, The adsorption of basic dyes from aqueous solution on modified-peat resin particle, *Water Res.* 37 (2003) 1535–1544.
- [29] V. Vimonses, S.M. Lei, B. Jin, C.W.K. Chow, C. Saint, Kinetic study and equilibrium isotherm analysis of Congo Red adsorption by clay materials, *Chem. Eng. J.* 148 (2009) 354–364.
- [30] Y.S. Ho, G. McKay, Pseudo-second order model for sorption processes, *Process Biochem.* 34 (1999) 451–465.
- [31] J.R. Weber, W.J. Morriss, Kinetics of adsorption on carbon from solution, *J. Sanit. Eng. Div. Am. Soc. Civ. Eng.* 89 (1963) 31–60.
- [32] S. Senthilkumar, P. Kalaamani, C.V. Subburaam, Liquid phase adsorption of crystal violet onto activated carbons derived from male flowers of coconut tree, *J. Hazard. Mater.* 136 (2006) 800–808.
- [33] M. Auta, B.H. Hameed, Optimized and functionalized paper sludge activated with potassium fluoride for single and binary adsorption of reactive dyes, *J. Ind. Eng. Chem.* 20 (2014) 830–840.
- [34] R. Wangpradit, P. Chitprasert, Chitosan-coated *Lentinus polychrous* Lév.: Integrated biosorption and biodegradation systems for decolorization of anionic reactive dyes, *Int. Biodeter. Biodegr.* 93 (2014) 168–176.
- [35] G. Sharma, M. Naushad, D. Pathania, A. Mittal, G.E. El-desoky, Modification of *Hibiscus cannabinus* fiber by graft copolymerization: Application for dye removal, *Desalin. Water Treat.* (2014) 1–8.